Advanced Fiber Materials (2024) 6:758–771
https://doi.org/10.1007/s42765-024-00388-7

RESEARCH ARTICLE

High-Performance Cellulose Nanofibers/Carbon Nanotubes Composite for Constructing Multifunctional Sensors and Wearable Electronics

Yali Liu[1,2] · Sufeng Zhang[1] · Lei Li[1] · Nan Li[1]

Received: 23 November 2023 / Accepted: 30 January 2024 / Published online: 14 March 2024

Abstract

The green preparation of highly dispersed carbon nanotube (CNT) conductive inks remains a critical challenge in the field of flexible electronics. Herein, a waterborne CNT dispersion approach mediated by carboxylated cellulose nanofibers (C-CNFs) was proposed. CNFs, special biomass materials with excellent nanostructures and abundant active surface groups, are used as green dispersants. During the dispersion process, benefiting from chemical charge and dimensional matching, C-CNF/CNT wicking-driven stable composite structures (CCNTs) were co-assembled via hydrogen bonding, electrostatic stabilization and π–π stacking between the interfaces, generating controlled orientational structures and promoting stable dispersion and conductivity of CNTs, which were demonstrated via molecular dynamics simulations combined with a variety of physicochemical characterization methods. The dispersion concentration of CNTs in a CCNT slurry can reach 80 wt%, and the obtained CCNT slurry has a low *zeta* potential (less than −60 mV) and good stability. Due to the film-forming properties of CNFs and in-plane oriented self-assembly of CCNT, the composite self-supporting films were fabricated with high electrical conductivity (67 S cm^{-1}) and mechanical performance (tensile strength of 153 MPa). In addition, the resulting biobased CCNT ink is compatible with a variety of printing processes and adaptable to various substrates. Moreover, this ink can be used to construct multifunctional advanced sensors with electrochemical, electrothermal, and deformation/piezoresistive responses, which demonstrate excellent performance in monitoring human health.

Keywords Carbon nanotubes (CNTs) · Cellulose nanofibers (CNFs) · Conductive inks · Dispersion · Printability · Multifunctional sensors

Introduction

The flexibility of electronic devices has become a key requirement for future smart electronics, including solar cells, displays, radio frequency identification, sensor tapes, capacitors and batteries [1]. Ink-based processes, which enable scalable fabrication of flexible devices based on nanomaterials, are practical approaches for producing wearable electronics [2, 3]. Due to their unique electrochemical activity, inherent mechanical strength, and high stability, CNTs are an ideal flexible, energetically active material for constructing wearable electronics [4, 5]. Currently, various CNT-based conductive slurries have been developed and successfully applied to the rapid and scalable fabrication of multifunctional flexible advanced equipment, such as flexible circuits [6, 7], sensors [8, 9], and energy equipment [10, 11]. However, CNTs tend to agglomerate into crystalline bundles because of the strong van der Waals attraction force and strong π–π interactions, which are important barriers to their chemical and physical manipulation and thus to their practical application [12, 13]. To overcome this barrier, advances in the maximum effective dispersion of CNTs in water and organic solvents while achieving their desired arrangement are critical for realizing many important commercial applications [14]. Currently, mechanical dispersion

✉ Sufeng Zhang
zhangsufeng@sust.edu.cn

1 College of Bioresources Chemical and Materials Engineering, Shaanxi University of Science and Technology, Shaanxi Provincial Key Laboratory of Papermaking Technology and Specialty Paper Development, Key Laboratory of Paper Based Functional Materials of China National Light Industry, National Demonstration Center for Experimental Light Chemistry Engineering Education, Xi'an 710021, China

2 Xinjiang Key Laboratory of Trace Chemicals Sensing, Xinjiang Technical Institute of Physics and Chemistry, Chinese Academy of Sciences, Ürümqi 830011, China

and functionalization are the main methods for dispersing CNTs [15]. Compared to the disadvantages of limited dispersion and unstable dispersion under pure mechanical dispersion [16], functional modification enhances the compatibility and stability between CNTs and dispersing solvents by introducing functional groups on the surface of CNTs or conducting physical adsorption and coating [17]. Functional modification is mainly achieved through two methods: covalent functionalization and noncovalent surface modification. In covalent functionalization, the hybridization of some carbon atoms on the sidewall of CNTs changes from sp^2 to sp^3, which changes the intrinsic properties of CNTs [18]. Noncovalent surface modification usually depends on adsorbing surfactant molecules on CNT surfaces to create hydrophilic–hydrophobic, π–π, or electrostatic interactions, which do not change the hybridization of carbon atoms and often retain the intrinsic physical and chemical properties of CNTs [19]. Herein, identifying a new functionalization method to improve the stability and dispersion of CNTs in solution and understanding the corresponding dispersion mechanisms are important for both practical applications and fundamental carbon science [20].

It was reported that high-content CNTs could be efficiently and stably dispersed in a CNF aqueous system. Furthermore, CNT–CNF composite fibres (1D) [21], films (2D) [22] and aerogels (3D) [23] can be directly constructed from CNT–CNF dispersions without additional extra structural materials. By combining the unique properties of cellulose nanofibers (lightweight, flexible, and humidity sensitive), CNT–CNF composite materials have been studied in depth in the fields of multifunctional sensors and flexible energy storage devices [24]. Increasing the CNT content is crucial for improving the application performance of CNT/CNF composite materials because of their high conductivity requirements [25]. It should be noted that the dispersion limit of nanocellulose to CNTs is determined by its surface charge density [26]. Hu et al. [27] used TEMPO-mediated CNFs with a high surface charge density to achieve a dispersion limit of 50% carboxyl-modified CNTs, which shows that there is still much room for improvement in the dispersion limit of CNTs. Hajian et al. [22] utilized TEMPO-mediated and acid-hydrolysed CNFs to achieve a dispersion limit of 75% CNTs. However, the dispersion was subjected to high-power ultrasound and ultraspeed centrifugation, which is a time-consuming and energy-consuming process. Thus, the development of CNFs with surface charges is a reasonable strategy for increasing the dispersion limit and ensuring the uniform and stable dispersion of CNTs to manufacture high-conductivity and flexible CNF–CNT materials.

In this study, we investigated the dispersion effects and mechanism of using C-CNFs as a green dispersant to disperse CNTs uniformly and stably in water. Furthermore, the performance of the CCNT dispersion system was verified by the application of the resulting biobased CCNT ink and conductive film in the field of flexible electronic and wearable sensing. Study results suggest that the regulation of chemical charge and dimensional matching enables the co-assembly of CCNT adhesive structures between C-CNFs and CNTs through hydrogen bonding, electrostatic interactions, and π–π stacking, promoting the stable mono-dispersion of CNTs without affecting their conductivity. Owing to the film-forming properties of CNFs and high CNT content, CCNT dispersions can independently form flexible self-supporting composite films with high electrical conductivity and excellent mechanical performance. It is of practical significance that the resulting CCNT dispersions exhibit compatibility with a variety of printing processes and adaptability to various substrates, allowing the architecture of multifunctional sensors with electrochemical, electrothermal, electrochemical and deformation/piezoresistive responses. Combined with the excellent biocompatibility of CNFs, these findings fully demonstrate the great potential of CCNT-based flexible electrodes in the field of smart wearable health monitoring and diagnostic devices.

Experimental Section

Chemicals and Materials

Unbleached kraft pulp (UBKP) was obtained from Tianjin Zhongchao Paper Co., Ltd. (Tianjin, China). Potassium permanganate ($KMnO_4$) and sulfuric acid (H_2SO_4, 98%) were obtained from Sinopharm Chemical Reagent Company (Shanghai, China). Commercially available multi-walled CNTs (95 wt% purity) were obtained from Nanjing XF NANO Materials Tech Co., Ltd. (Nanjing, China). The CNTs are 10–30 μm in length and 10–20 nm in diameter. Other materials were purchased from commercial suppliers and can be used without further treatment.

Isolation of C-CNFs and CCNT Slurry Preparation

C-CNFs were obtained using our previously developed potassium permanganate oxidation method and stored at 4 °C for backup [28, 29]. The prepared C-CNF suspension was diluted to 1 mg mL^{-1} (the concentration used in all the dispersion preparations), and a certain amount of CNT powder was added and then sonicated (650 W, 20 min) in an ice-water bath (JY99-IIDN, Jingxin, China) to obtain a CCNT slurry with mass ratios of C-CNFs to CNTs of 1:9, 2:8, 3:7, 4:6, 5:5 and 6:4, all of which had the same particle concentration (4 mg mL^{-1}). The obtained slurries were denoted as $CCNT_{1/9}$, $CCNT_{2/8}$, $CCNT_{3/7}$, $CCNT_{4/6}$, $CCNT_{5/5}$, and $CCNT_{6/4}$. The preparation of CCNT ink is described in the Supplementary Information.

Molecular Dynamics Simulation

The carbon nanotube (CNT) model was built by VMD 1.9.4 [30]. The native cellulose nanofibril (CNF) model was constructed from glucan chains, each with 8 glucose units; this is currently the most accepted model [31]. Every other glucose unit in the surface chains was substituted for a glucuronic acid unit to represent highly oxidized C-CNFs. Carboxyl groups were arranged such that they were all exposed to the outside of the crystal. Chains in the centre of the C-CNF crystal remained chemically identical to those of the CNFs.

The MD simulations reported here were conducted by using the GROMACS 2019.6 simulation package [32] with a basic time step of 2 fs. The nonbonded interactions used a cutoff distance of 1.2 nm, and long-range electrostatic interactions were employed using PME. [33]The GLYCAM_06j [34]parameters were used for carbohydrate analysis combined with GAFF [35] for CNTs and the TIP3P [36]water model. CNT molecules were frozen in the Y direction during the 20 ns simulation.

Construction of CCNT Composite Films

A certain amount of prepared CCNT slurry with different ratios (ratios of C-CNFs to CNTs of 1:9, 2:8, 3:7, 4:6, 5:5 and 6:4) was filtered to form a film, and after the film was formed, it was dried in a vacuum drying oven (60 °C, 2 h) to obtain CCNT films with the same quantity (0.003 g cm^{-2}).

Assembly of CCNT-Based Flexible Capacitors

The electrodes of the capacitors were fork-finger electrodes obtained by stencil printing on plastic with a CCNT slurry. The gel electrolyte was prepared by dissolving agarose (1.5 wt%) in boiling standard phosphate-buffered salt solution (PBS) and cooling to room temperature. The gel electrolyte was introduced into the container with fork-finger electrodes while being hot, cooled, and shaped to obtain a flexible capacitor, which was subsequently encapsulated and used for electrochemical performance testing.

Preparation of the Deformation/Pressure Sensors

Conductive filter paper (CCNT/FP) was cut into specimens (10 mm × 30 mm), wound with wires, and then attached to insulating transparent tape to make sensors.

Electrothermal Response of CCNT/FP

With the assistance of infrared thermography (SYSTEMS-INC, FLIR, USA), the electrothermal response characteristics of each CCNT/FP sensor (3 cm × 1.5 cm) were demonstrated at a range of voltages provided by a regulated power supply.

Electrochemical Performance of CCNT-Based Flexible Capacitors

Cyclic voltammograms of the capacitors at different scanning rates (5 mV s^{-1}, 10 mV s^{-1}, 20 mV s^{-1}, 50 mV s^{-1}, and 100 mV s^{-1}) and certain bending deformations were recorded via cyclic voltammetry (CV) by an electrochemical workstation (CHI660e, Chenhua, China). The capacitor area over capacitance calculations is detailed in the Supplementary Information.

Deformation/Pressure Sensing Behaviours of CCNT/FP Electrodes

The instrument used to test the resistance changes induced by deformation/tiny signals from pressure and human movement in the CCNT/FP-based electrodes was a digital bridge (TH2829A, Tonghui, China). After connecting the device, the volunteers wearing the sensors performed corresponding movements or performed the corresponding actions. This part of the experiment was completed with the assistance of two volunteers, and informed written consent was obtained for publishing the images and data. This study was approved by the Institutional Ethics Committee.

The other experimental details are provided in the Supplementary Information.

Results and Discussion

Stably Dispersed CCNT Slurries: Preparation and Characterization

Figure 1 illustrates the preparation and properties of the CCNT dispersion. The CNTs were successfully dispersed in water, which was attributed to the assistance of C-CNFs by regulating interfacial interactions. C-CNFs with high carboxylate content were obtained via potassium permanganate oxidation in conjunction with a slight mechanical process and used as an efficient green surfactant to disperse CNTs (Fig. 1a, b). Notably, CCNT dispersions remain highly stable and can be stored for months without precipitates (Fig. S1, Supplementary Information). The prepared CCNT slurry droplets can be dispersed rapidly in water without any visible agglomeration (Fig. 1c) compared with those of pure CNTs (Fig. S2, Supplementary Information), which also demonstrates the good dispersion of the CCNT slurry. Quantitatively, we evaluated the stability of CCNT slurries using a multiple light diffractometer (MLD) to explore the effect of different C-CNF and CNT mass ratios on the stability

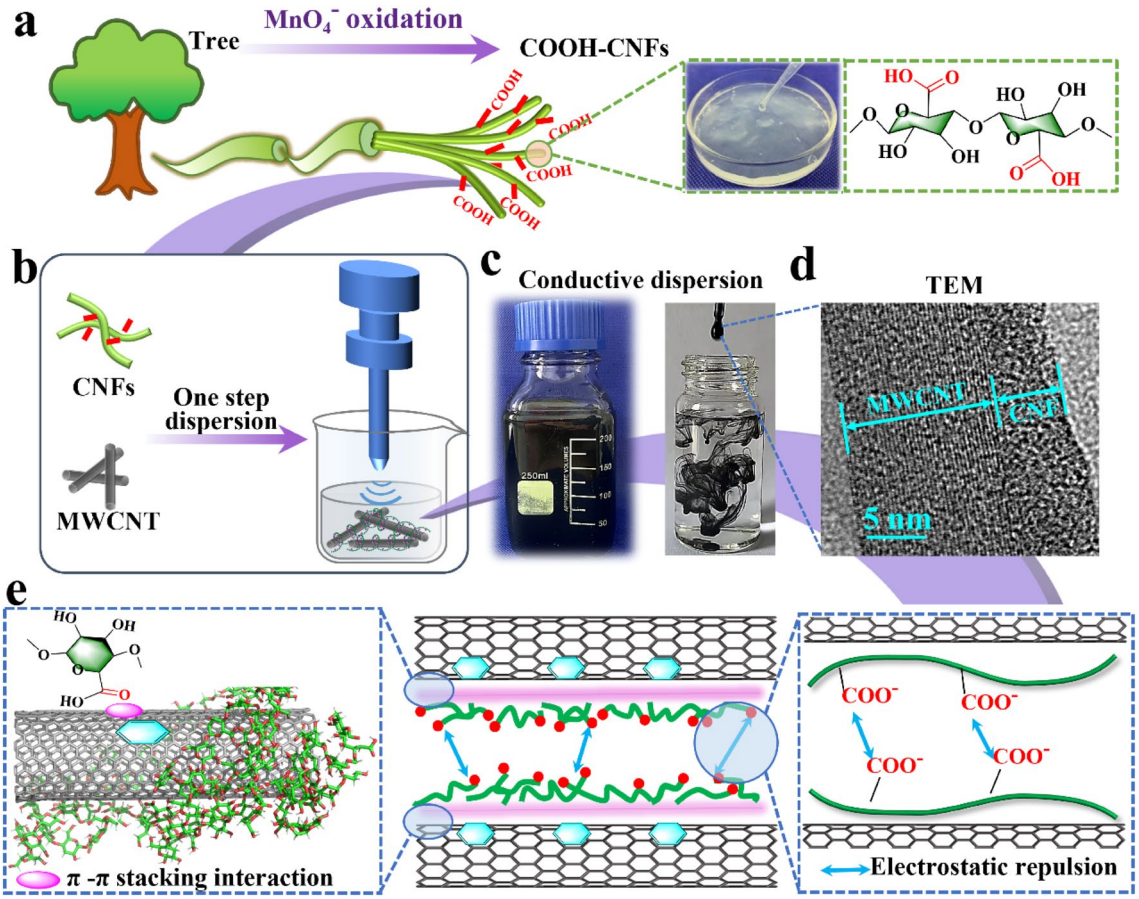

Fig. 1 Preparation and characterization of the CCNT dispersion. **a** Schematic illustration showing the extraction of C-CNFs. **b** Schematic illustration showing the formation of a CCNT slurry. **c** Digital photographs showing the rapid spreading of CCNT ink in water. **d** TEM images of the CCNT slurry. **e** Dispersion mechanism based on the π–π conjugate effect and coordination of electrostatic repulsion between C-CNFs and CNT molecules

of CCNT slurries, obtaining the stability index, TSI, calculated from the transmission spectra of different CCNT slurries in the analyser. The TSI is a measure of the stability of the nanosuspension, and the TSI of all CCNT slurries is less than 0.06 (Fig. S3, Supplementary Information), which quantitatively verifies the stability of this system [37]. The adhesion structure of the CCNT hybrids can be visualized by high-resolution TEM images. The internal crystalline part and the external amorphous part can be clearly distinguished (Fig. 1d), which can be attributed to the multiple walls of the CNTs and the surface-adhered C-CNFs, respectively.

A series of measurements and characterizations were used to analyse the surface properties of the CCNT slurry, with the *zeta* potential being the first parameter to be measured. According to ASTM standards, the criterion for ''good stability" requires a *zeta* potential above (+ or −) 40 mV [38]. The *zeta* potentials of the CCNT slurry and the control group (C-CNF solution) were − 72.4 and − 53.3 mV, respectively (Fig. S4, Supplementary Information), which could be attributed to the change in the shear surface of the water outside the C-CNFs when the C-CNFs contacted the CNTs [25]. Moreover, the negative potential of C-CNF was sufficient to maintain the uniformity and stability of the CCNT slurry at the high dispersion limit of CNTs, which can be effectively proven by the typical Tyndall effect (inset in Fig. S4, Supplementary Information). The above results demonstrate that the effective dispersion of CNTs mediated by C-CNFs can be attributed to three main factors (Fig. 1e): (i) aggregation between CNTs via π–π stacking is disrupted by ultrasonication, which is an important prerequisite for ensuring interactions between C-CNFs and CNTs [22]. (ii) With the assistance of ultrasound, the CNTs were pushed towards the C-CNFs and localized in the effectively charged –COOH region on the surface of the C-CNFs. Next, the interaction between the two nanomaterials via noncovalent π–π stacking is induced by the sp^2 carbon lattice [22, 39], yielding C-CNF-modified CNTs with high charges and steric effects on the surface, which effectively prevent recombination between CNTs in the structure [40]. (iii) In addition, the hydrogen

bonding between CNTs and C-CNFs may be conducive to the dispersive stability of CCNT.

We investigated the intermolecular interactions between C-CNFs and CNTs via X-ray diffraction (XRD), Raman spectroscopy, FT-IR spectroscopy and XPS. The CNTs had sharp and weak diffraction peaks at 25.7° and 43.2°, respectively, which are attributed to the (002) and (100) crystal planes, respectively, and the crystallinity was calculated to be 96.16% (Fig. 2a). The CCNT conductive films showed two characteristic diffraction peaks at 2θ values of 15.5° and 22.8°, which corresponded to the overlap of the (1–10)/(110) crystallographic plane and the (002) crystallographic plane on the C-CNFs, respectively, revealing the typical cellulose I crystalline structure and indicating that the addition of CNTs did not change the crystal structure of the C-CNFs [29]. With increasing CNT content in the composite system, the crystallization indices of the CCNT conductive films increase overall (from 70.56 to 76.38%) (Fig. S5, Supplementary Information). This could be attributed to the heterogeneous nucleation effect induced by CNTs in the composite system, which induces C-CNFs to adsorb on its surface, promoting the nucleation process of C-CNFs at the interface between CNTs and C-CNFs and accordingly improving the crystallization index of the C-CNF matrix [41]. Moreover, the enhanced interfacial interaction between CNTs and C-CNFs also contributes to the mechanical strength of CCNT conductive films. As shown by Raman spectroscopy (Fig. 2b), the presence of typical absorption peaks of cellulose can be observed in the C-CNF spectrum. The peak attributed to CNTs at 1346 cm^{-1} corresponds to the D band, and the peaks at 1579 cm^{-1} and 2690 cm^{-1} denote the G and 2D bands, respectively [42]. For CNT-based electrode materials, the larger the I_D/I_G is, the higher the electron conduction efficiency and the better the cycling efficiency of the electrode [43]. With increasing C-CNF addition, the I_D/I_G ratio of the composite conductive film gradually increases, indicating that the C-CNFs adhere to the surface of the CNTs, causing additional defects on the surface of the CNTs. This structure endows the composite conductive film with higher electrical conductivity and thermal conductivity [44], which lays a favourable foundation for the application of CCNT-based electrodes in energy storage and thermal management devices.

FT-IR characterization and XPS analysis of different CCNT composite conductive films were carried out to further reveal the interactions between CNTs and C-CNFs in this study. There are no obvious absorption peaks in the CNT FT-IR spectra (Fig. 2c), indicating that no other functional groups exist on the CNT surface, while the C-CNF films show characteristic peaks for cellulose, except for a characteristic peak for the stretching vibration of C=O at 1730 cm^{-1}, confirming the existence of –COOH groups [28]. The CCNT composite conductive films with different C-CNF additions exhibited similar characteristic peaks of cellulose. With increasing CNT content, the intensity of the cellulose characteristic peaks in the FT-IR spectra of the CCNT composite conductive films decreased, which laterally reflected the interactions between the C-CNFs and

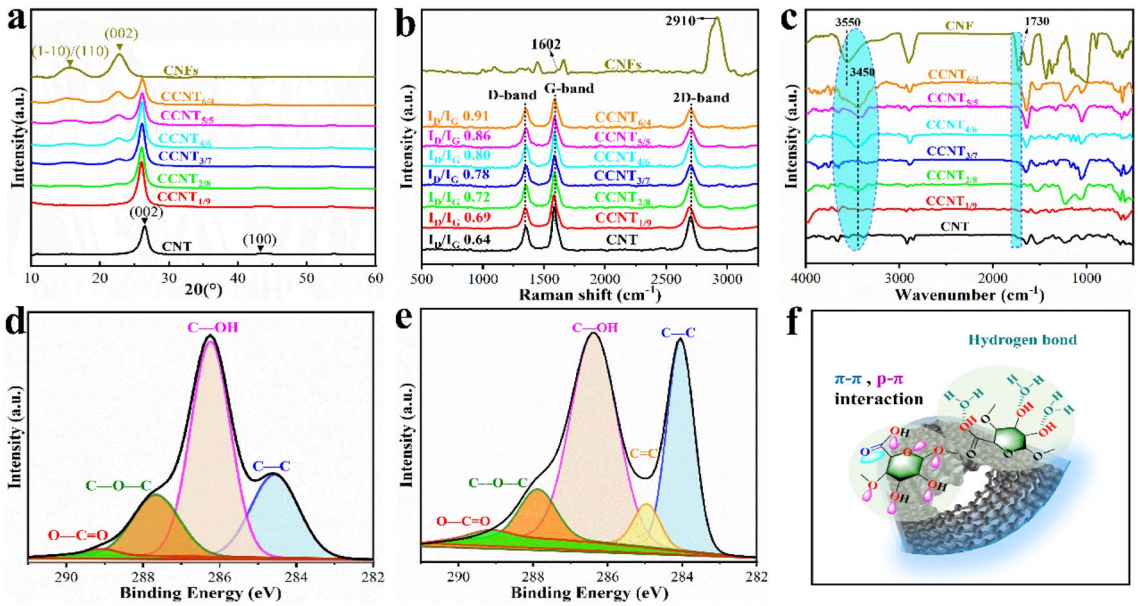

Fig. 2 Interaction between C-CNFs and CNTs. **a** XRD patterns of CNF, CNT and CCNT films. **b** Raman spectra of CNF, CNT, and CCNT films. **c** FT-IR spectra of CNF, CNT, and CCNT films. **d** High-resolution C1s XPS spectra of the pure CNF film and **e** CCNT composite film. **f** Scheme of the interfacial interaction between C-CNFs and CNTs

CNTs. Notably, compared with the FT-IR spectra of the pure C-CNF films, the –OH stretching vibration peak of the CCNT composite conductive films shifted to a lower frequency from 3550 cm^{-1} to approximately 3450 cm^{-1}. Combined with the disappearance of the characteristic absorption peak of the carboxylate group of C-CNFs at 1730 cm^{-1} in the CCNT composite conductive film, the occurrence of hydrogen bonding interactions between C-CNFs and CNTs was well proven [45]. High-resolution C1*s* XPS spectra of the pure C-CNF films and CCNT composite conductive films are shown in Fig. 2d, e. The C–C, C–OH, C–O–C and O–C=O bonds in the CNF films correspond to the peaks at 284.8 eV, 286.2 eV, 287.3 eV and 288.8 eV, respectively, while in the CCNT composite conductive films, they correspond to 284.6 eV, 286.6 eV, 288.0 eV and 289.1 eV, respectively. The binding energies corresponding to the C–OH, C–O–C and O–C=O peaks of the CCNT films are greater than those of the pure C-CNF films, which can be attributed to the hydrogen bonding interactions between the CNTs and CNFs [46]. In addition, the fractional peak at 285.1 eV for the CCNT films is characteristic of C=C bonding formed by π–π stacking of the carbon lattice sp^2 in the CNTs with the carboxyl groups in the C-CNF molecules, which further reveals the interactions between CNTs and CNFs. In summary, ultrasonic-assisted supramolecular co-assembly between C-CNFs and CNTs was realized mainly through hydrogen bonding and π–π stacking interactions (Fig. 2f), and ultimately, CCNT hybrids with C-CNFs adhered to the surface of CNTs were obtained.

To verify the effect of ultrasonic assistance, we compared the dispersion state with and without ultrasound. In contrast, magnetic stirring could not provide enough energy to disrupt the π–π interactions between CNTs; even with prolonged stirring, a homogeneously dispersed slurry could not be obtained, and significant delamination was observed (Fig. S6, Supplementary Information). This indicates that the C-CNFs could be effectively dispersed in water by ultrasonication, which can be explained by the fact that the bubble cavitation generated during ultrasonic treatment usually provides enough energy to destroy the aggregates via π–π stacking interactions between CNTs in water [47]. Aggregation of unstably dispersed CNTs occurs rapidly once ultrasonic treatment is terminated [48]. In the presence of C-CNFs, CNTs were pushed towards the effectively charged regions of the surface of the nanocellulose and bound to these highly charged materials, preventing reaggregation through electrostatic repulsion. However, studies and calculations of the quantitative relationships of interactions between the interfaces of CNTs and CNFs are lacking [49]. Molecular dynamics (MD) simulations were performed to further investigate the formation mechanism of the CCNT complex (the water model is shown in Fig. S7, Supplementary Information). To simplify the simulations without eliminating the essential features of interactions between C-CNFs and CNTs, a representative fragment of C-CNFs was used (Fig. 3a), where every other glucose unit in the surface chain in the model was replaced by a glucuronic acid unit, representing highly oxidized C-CNFs. Figure 3b shows snapshots of the CCNT system at 0, 5, and 20 ns, where water and ions are hidden. Under steric hindrance, the carboxyl group at C6 in the C-CNFs was exposed and arranged outside the cellulose molecule, and the C-CNFs gradually approached the CNT surface under the facilitation of the carboxyl group. Notably, the C-CNFs were in contact with the CNT surface for approximately 5 ns and then "stuck" on the surface until the end of the simulation, and the 5 ns phase was defined as a transition state considering the conformational changes during this process. The detailed distribution histograms and predicted densities of atoms in the C-CNF molecule in the initial, transition and final states show a slight shift in the distance distribution towards the shrinkage point, which suggests that the C-CNFs were close to the CNT surface (Fig. 3c). Snapshots near CNTs and C-CNFs show that the distance between the two materials rapidly decreases to ~0.4 nm, while the angle stabilizes at ~0° (Fig. 3d), indicating strong π–π interactions between the C-CNFs and CNTs via surface carboxyl groups. As the simulation time progresses, the two molecules stabilize at a distance, and the average binding energy decreases to -353.18 $kJ{\cdot}mol^{-1}$ (Fig. 3e, f). The binding energy is the manifestation of intermolecular attraction, which indicates that the noncovalent π–π stacking and hydrogen bonding between C-CNFs and CNTs are spontaneous processes. According to the energy minimum principle, the lower the energy, the greater the stability of the system [50]. This result quantitatively verifies the rationality of the previously proposed mechanism in which C-CNFs, as dispersants, effectively improve the dispersion of CNTs in water.

Performance Characterization of CCNT Composite Conductive Films

CCNT films with neat and dense layer-by-layer cross sections (Fig. 4a) were obtained by completing the in-plane oriented self-assembly of the CCNT slurry driven by evaporation and vacuum filtration, which facilitated directional electron transport and mechanical strength [51] (Fig. 4b). Figure 4c shows a schematic representation of the CCNT in-plane oriented self-assembly film formed via vacuum suction. With increasing C-CNF content, the CNTs were clearly encapsulated by C-CNFs and co-assembled into relatively flat and dense surfaces (Fig. S8, Supplementary Information) and cross sections (Fig. S9, Supplementary Information) via hydrogen bonding. This structure provides good conductive transport channels and excellent mechanical strength for CCNT composite conductive films [52], which

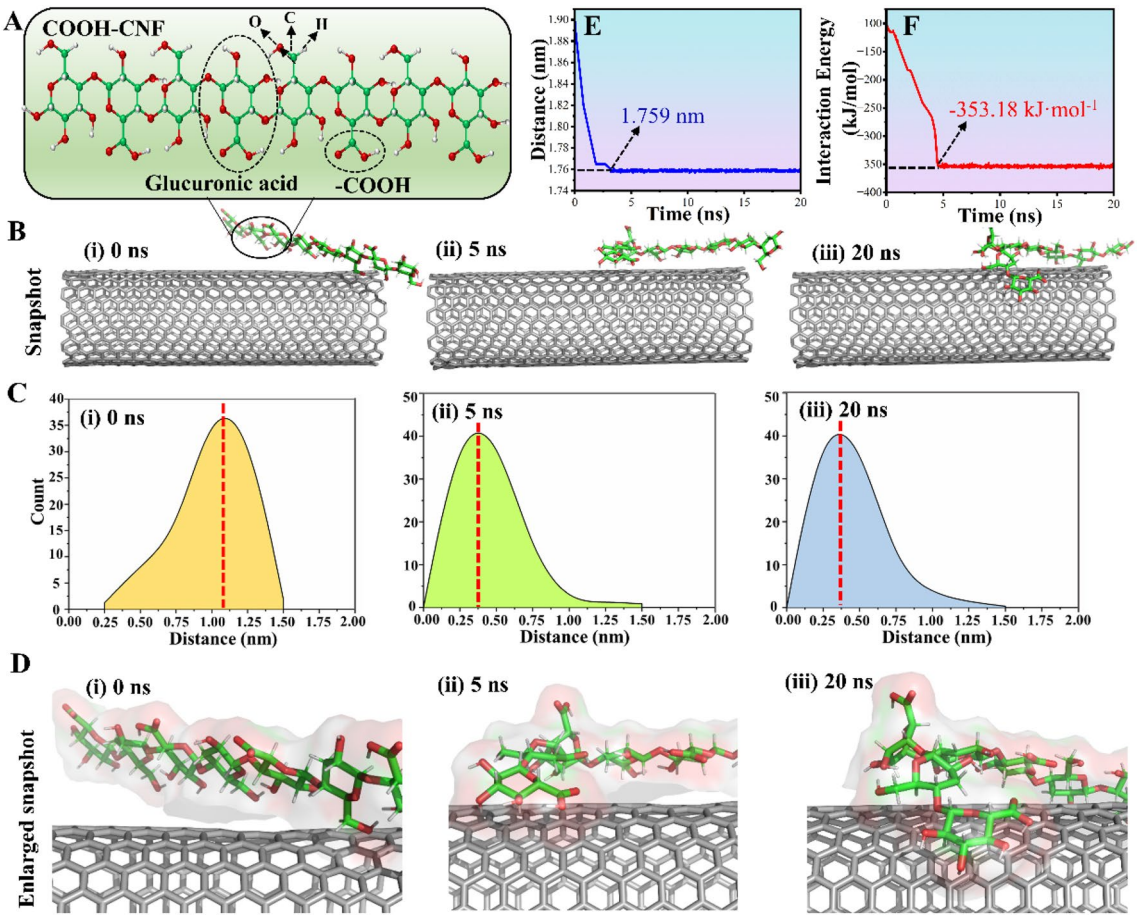

Fig. 3 Molecular dynamics simulation results of C-CNF and CNT interactions. **a** Model of C-CNFs: every other glucose unit in the surface chain was replaced by a glucuronic acid unit, representing highly oxidized C-CNFs. The carboxyl groups are arranged so that they are all exposed on the outside of the crystal; **b** snapshots of the system at 0, 5 and 20 ns. Water and ions are both hidden; **c** histogram and estimated density of the distance between C-CNFs and the CNT surface at 0, 5 and 20 ns; **d** snapshot around the carboxyl group of C-CNFs. **e**, **f** are the distance and energy, respectively, between the C-CNFs and CNT molecules at 0–20 s

well explains the phenomenon of decreasing film thickness and increasing compactness with increasing C-CNF content at the same dosage (0.003 g cm^{-2}) (Fig. S10, Supplementary Information).

Figure 4d illustrates the trend of the mechanical properties of CCNT composite conductive films with different CNT contents. When only a small amount of CNTs (approximately less than 70 wt%) was added, the tensile modulus and stress increased significantly, the stress in the film reached 152.87 MPa, and the Young's modulus was 5.26 GPa when the CNT content was 40 wt%. In comparison, pure CNTs were unable to form a film under the same treatment conditions, and the stress in the pure C-CNF film was 75 MPa. This may be attributed to the fact that the C-CNF and CNT molecules in the slurry come close to each other during filtration, and an encapsulated coassembled structure was constructed under the synergistic effect of carboxyl group induction and site-blocking effects, which endows the composite conductive film with excellent mechanical strength/toughness and electrical conductivity. Specifically, the good dimensional matching between the two materials, both of which have high aspect ratios, induces the two to become entangled with each other, which is subsequently enhanced by π–π stacking and intermolecular hydrogen-bonding interactions, ultimately leading to the formation of high-strength composite conductive films [53]. As the weight content of the CNTs increases further (> 70 wt%), the stress and Young's modulus of the films decrease dramatically, mainly because the CNT content exceeds the dispersion limit of the C-CNFs in the system, and CNTs cannot be effectively dispersed, which also destroys the network structure of the C-CNF films. Then, the C-CNFs adsorb on the surface of the CNTs agglomerate and settle together, and the structure of the film becomes looser (which again verifies the rule of change in the film tightness and the SEM image of the film cross section), leading to a decrease in

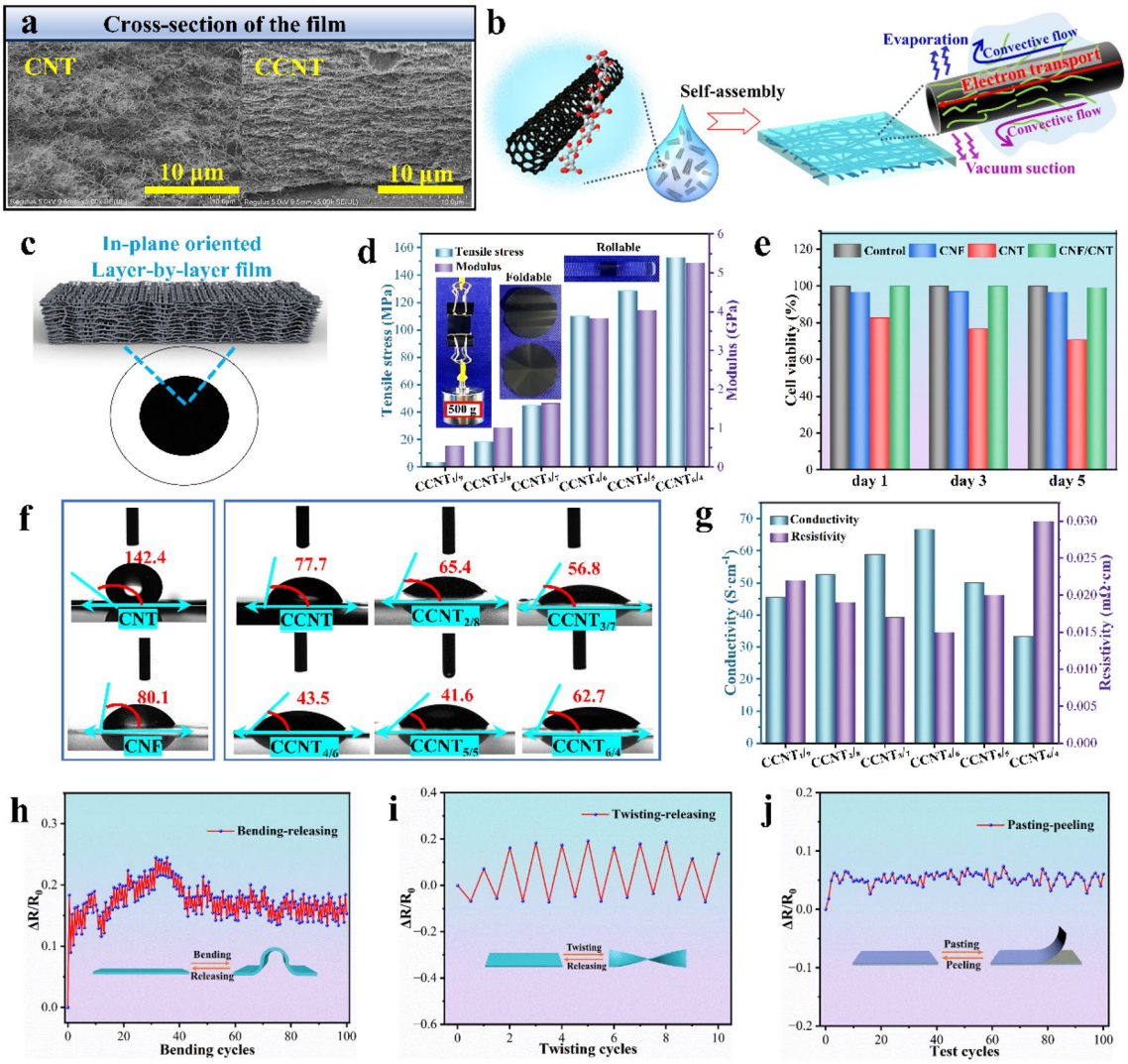

Fig. 4 Characterization of free-standing CCNT films. **a** Cross-sectional morphology of the films. **b** Schematic depiction of the evaporation and vacuum filtration-driven self-assembly of CCNT. **c** Schematic representation of self-assembled CCNT films with an in-plane orientation. **d** Mechanical property analysis of different CCNT composite films. **e** Cell viability in different groups on different culture days. **f** Water contact angles of the CNT, CNF and CCNT films. **g** Conductivity and resistivity of different CCNT films. **h–j** Changes in the resistance of the film after 500 bending cycles, 10 twisting cycles and 100 tape peeling cycles

strain, increase in brittleness and decrease in the mechanical properties of the composite conductive film. With a further increase in the weight of the carbon nanotubes (more than 70 wt%), the stress and Young's modulus of the films decreased dramatically, mainly because the content of the carbon nanotubes exceeded the dispersion limit of the C-CNFs in the system, and an ordered coassembled structure could not be formed between the CNTs and the C-CNFs. The above results indicate that the dispersant limit of CNTs in this system is between 70 and 80 wt%, which is consistent with the previous results of dispersion stability analysis of CCNT slurries. The CCNT composite conductive film can withstand a weight of 500 g without any cracks or breaks and can withstand multiple bending and folding cycles, all of which indicate that it has excellent mechanical properties (inset of Fig. 4d).

Figure 4e shows the graph of the cell viability assay data for the mouse fibroblast L929 cell line after incubation in dishes coated with CNFs, CNTs or CCNT for 1–5 days. The cellular activity of the L929 cells in the CCNT group was comparable to that of the control group, indicating that the CCNT slurry has long-term cytocompatibility and is slightly more compatible than the CNF component; thus, the combination of CNFs and CNTs promotes the growth of L929 cells. This difference may be attributed to the fact that, compared to the dense structure of the pure CNF film, the conductive CCNT composite film has a looser structure, which can deliver sufficient oxygen and nutrients for

cell growth. In contrast, the lowest activity of L929 cells in the CNT group gradually decreased with increasing culture time, showing that CNTs have certain cytotoxicity. The live/dead fluorescence assay provides a quick method for assessing the proportion of live and dead cells in cell culture systems, by which the biocompatibility of the three components of CNFs, CNTs and CCNT was more clearly demonstrated (Fig. S11, Supplementary Information). These results indicated that CCNT is a safer choice for preparing slurries for printing and wearable electronics than conventional CNT surfactants because of its potential cytotoxicity.

Next, the hydrophilicity of the C-CNF, CNT and CCNT films was analysed by instantly acquiring water contact angle (WCA) images. The high hydrophobicity of the CNTs was confirmed by the WCA (142.4°) of the bare CNT film (Fig. 4f). C-CNFs are inherently hydrophilic, while the corresponding films have a high WCA (80.1°), which is attributed to their dense, smooth surface and high barrier properties [54]. The WCA of the CCNT composite conductive films varies with increasing C-CNF content, showing a decreasing and then increasing trend. The hydrophobicity of CNTs can be improved by the addition of a small amount (10–50 wt%) of C-CNFs on the surface, which makes the composite conductive film hydrophilic, and when the content of C-CNFs in the system is greater than 50 wt%, dense and smooth C-CNF films are constructed on the surface of the CNTs, which increases the water contact angle. Based on the surface carboxylate structure, hydrophilic C-CNFs adhered to the CNT surface via π–π bond interactions, realizing hydrophilic modification of the original hydrophobic structure of the CNTs. The hydrophilic modification of CNTs by C-CNFs is highly important; e.g., this modification improves the compatibility of CCNT conductive slurries with a variety of substrates, and it is expected that hydrophilic-modified CNTs will be useful in water-responsive actuators [55].

The conductivity and resistivity of the CCNT composite conductive films varied with the mass ratio of CNTs to C-CNFs (Fig. 4g). With increasing C-CNF addition in the system, the conductivity of the CCNT composite conductive films tended to increase and then decrease, while the resistivity showed the opposite trend. When the concentration of C-CNF increased from 10 to 40 wt%, the conductivity of the CCNT films increased significantly to 67 S cm^{-1} with a resistivity as low as 0.015 mΩ cm. This is closely related to the dispersing effect of the CCNT slurry, which, as discussed before, has a better dispersing effect on the CNTs when the C-CNF additions are in the range of 10–40 wt%. When the amount of C-CNF added is greater than 40 wt%, the conductivity of the resulting composite conductive film decreases accordingly, which is detrimental to the conductive material.

Through the above comprehensive study on the physicochemical properties of CCNT composite conductive films, combined with the findings of previous studies on the properties of CCNT slurries, the optimal conditions for this CCNT composite system were determined to be a mass ratio of C-CNFs to CNTs of 4:6, i.e., $CCNT_{4/6.}$ By comparison to the reported works, in this work, we found that the one-step dispersion of CNTs using biobased C-CNFs as a green dispersant is more efficient and less time-consuming than the other methods, and the supramolecular coassembly of C-CNFs and CNTs in this system and the high dispersion concentration endow the films with excellent mechanical properties and electrical conductivity (Table S1, Supplementary Information). More importantly, this work thoroughly studied the dispersion mechanism of CNTs on CNFs, which provides a sufficient theoretical basis and experimental foundation for the construction and application of carbon-based functional composite systems.

In practical applications, the conductive stability of conductive films is an important condition for ensuring that they can be used for a long period of time [56]. The stability of the $CCNT_{4/6}$ conductive films was confirmed by examining the changes in resistance during 500 bending cycles, 10 torsion cycles, and 100 tape stripping cycles (Fig. 4h–j). After 500 bending cycles, the resistance change in the CCNT composite conductive film is less than 0.2; after 10 twisting cycles, the resistance change in the CCNT composite conductive film is approximately 0.2; after 100 tape stripping cycles, the resistance change in the CCNT composite conductive film is less than 0.1. The CCNT composite conductive film prepared in this study under various deformations still exhibited excellent mechanical and conductive properties under various deformations. This difference is attributed to the efficient dispersion of CNTs by C-CNFs and the abundant hydrogen bonding in the vacuum-assisted self-assembled film structure [57]. Notably, circuits based on composite conductive films with different deformations of CCNT can make light-emitting diode (LED) bulbs (Fig. S12, Supplementary Information), which indicates that the composite conductive films have good conductive stability for coping with various extreme deformations. In conclusion, the excellent conductivity, and mechanical properties of CCNT composite conductive films can meet the needs of multifunctional applications.

Development and Application of CCNT Conductive Ink-Based Flexible Electrodes

The 0.5 wt% solid content of the conductive ink between the fluid and solid states can be adjusted by adjusting the shear angle frequency (Fig. S13, Supplementary Information, for its rheological properties), and this CCNT conductive ink is suitable for application in the fabrication of printed/written circuits. We demonstrated a CCNT ink-based writable conductive pen that writes on printing paper to obtain

a conductive line with a resistance of 6.5 kΩ (Fig. S14, Supplementary Information), which can light up an LED bulb (Fig. 5a). We demonstrate a CCNT ink-based conductive pen that writes on printer paper to obtain a conductive line with a resistance value of 6.5 kΩ. that lights up an LED bulb. This difference is attributed to the excellent hydrophilicity of the CCNT ink. After writing, the ink in the C-CNF and CNT components and paper surface cellulose easily combine through hydrogen bonding, which is conducive to the construction of conductive pathways. Screen printing has the advantages of simple equipment, easy operation, easy and inexpensive printing, plate making, high adaptability, and, most importantly, patterned design. Patterned electrodes were prepared using screen printing, and their conductive properties were investigated (Fig. 5b). The patterned conductive lines were prepared by customized stencils, and the CCNT ink was transferred well to the paper surface during the printing process. All three LED bulbs of different colours were successfully lit by connecting the dried conductive circuits, with a regulated voltage of 3 V. Conductive fabric and conductive filter paper filters were obtained by impregnating the CCNT ink to increase the conductivity of the fabric and filter paper, which could light up the LED bulbs (Fig. 5c). The effects of the number of impregnation cycles on the surface morphology (Fig. S15, Supplementary Information), mechanical properties, and electrical conductivity (Fig. S16, Supplementary Information) of the conductive filter paper were explored, and three impregnation-curing treatments of the FPs were optimized considering the production costs and economic benefits. Conductive modification of PVDF, cotton fabric and paper surfaces can be achieved by simple coating because the hydrophilic structure of CCNT

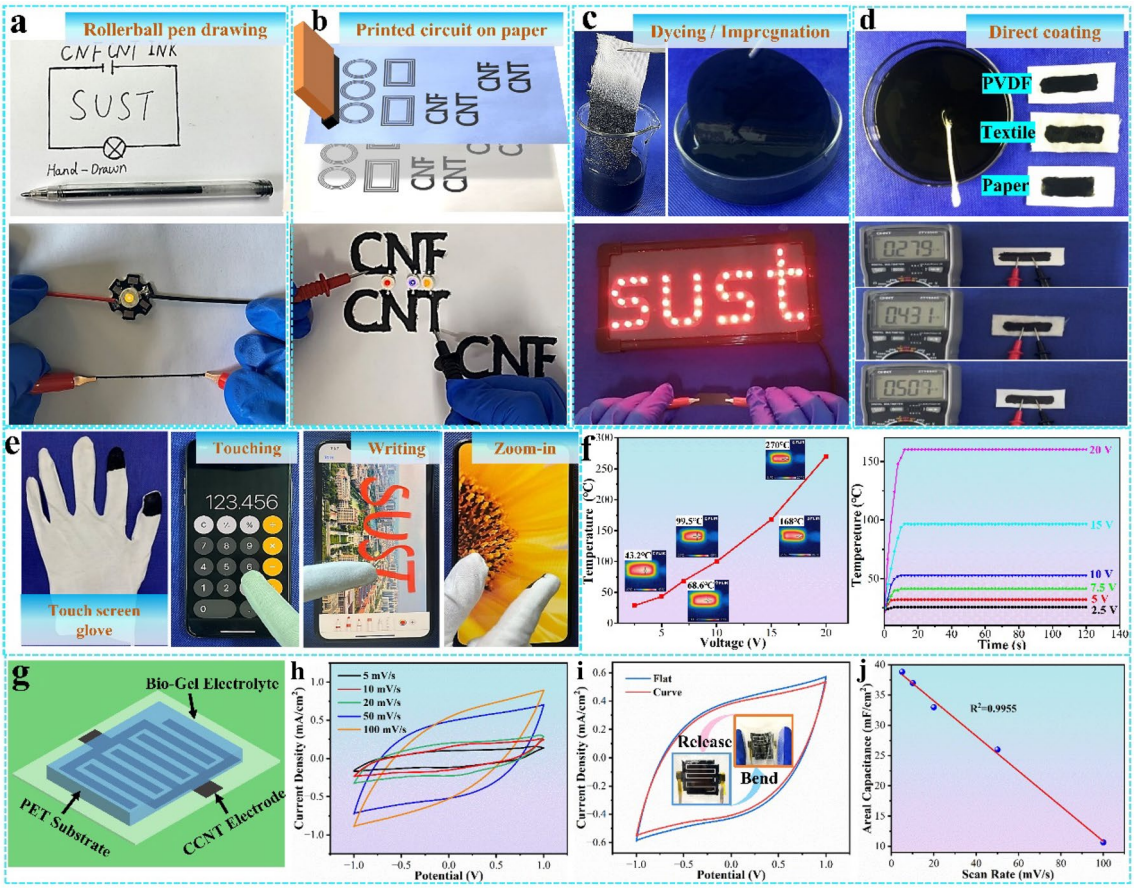

Fig. 5 Application of the CCNT ink. **a** Paper-based circuits prepared via rollerball pen drawing (upper) and photographs of an LED connected to the circuits (lower). **b** Schematic of the screen-printing process (upper) and photographs of an LED connected to a circuit (lower). **c** Schematic diagram showing the fabrication of CCNT-based conductive textiles (upper) and photographs of an LED connected to the circuits (lower). **d** Photographs of inks printed on paper, textile and PVDF substrates and their resistance. (e) Photographs of a touch screen glove made of CCNT and an operating smartphone, e.g., touching, writing, and zooming in, respectively (from left to right). **f** Electric heating property and thermal stability performance of the CCNT-based sensor. Electric heating property of the CCNT-based sensor under various voltages and electric heating curve for the CCNT-based sensor under various voltages. **g–j** Characterization of the CCNT-based flexible capacitor, e.g., schematic diagram of the CCNT-based capacitor, cyclic voltammograms of the capacitor at different scan rates and at flat and curved states and calculated areal specific capacitance at different scan rates

conductive inks ensures good adhesion to the substrate materials (Fig. 5d). The resistances of the electrodes coated on the PVDF, fabric and paper substrate materials were measured with a hand-held multimeter and were 0.279, 0.431 and 0.507 kΩ, respectively, and the differences in resistance appeared to be related to the surface and internal structure of the substrates.

E-textiles are an emerging development and are regarded as an important basic unit for building a new generation of wearable fabric-based electronics [58]. Smartphones can be smoothly operated by conductive gloves functionalized with CCNT ink, such as writing, touch scrolling, or two-finger zooming gestures (Fig. 5e). With the excellent electrical and thermal properties of CNTs, composite conductive filter paper can be used as a sensor to show great potential in terms of electrical and thermal performance and thermal stability. The heating capacity of the sensor increases significantly when the applied voltage is increased from 2.5 to 20 V (Fig. 5f), which matches the characteristics of electrically heated materials in practical applications [59]. Moreover, all the samples had a thermal response time of less than 15 s and reached a stable temperature with a high stability of 2 min. A point worth emphasizing is that a thermotherapy operating temperature of 42 °C for local heating of the human body can be achieved in the voltage range of 5–7.5 V. To achieve real-time monitoring of changes in the skin and avoid burns [60], conductive filter paper, therefore, has great potential for application in the field of wearable thermotherapy technology. To assess the potential of ink-based electrodes as electrochemical devices such as capacitors and biosensors, cyclic voltammetry (CV) was performed with CCNT-based flexible electrode patterns in biological media to confirm their electroactivity. The prepared capacitor showed a stable high area specific capacitance of 26 mF cm^{-2} at a sweep speed of 50 mV s^{-1} (Fig. 5g). In addition, capacitors with good flexibility can still maintain good electrochemical performance under bending deformation, and the cyclic voltammetry curves of the devices in the flat and bent states are shown in Fig. 5h–j. Benefiting from their biocompatibility and good flexibility, such capacitors have potential applications in biological systems.

Flexible Conductive CCNT-Based Films for Wearable Strain/Pressure Sensors

CCNT/FP was prepared with filter paper as a template, which retains a large number of distributed pores and high porosity within the filter paper; in addition, the resulting material has good electrical conductivity and good mechanical properties and thus can be applied to other sensors [61]. The resistance of the pressure sensor varies regularly during finger pressing and walking, providing real-time activity information about the finger and foot (Fig. 6a, b). In addition, the sensor also exhibits a stable and repeatable sensing signal for the action of clenching a fist when the sensor is adhered to the wrist, and an immediate sensing property for each flexion of the finger joint (Fig. 6c–e). Surprisingly, the sensor exhibited a sensitive response characteristic for monitoring subtle body signals, including swallowing, speaking, pulse, and breathing (Fig. 6f–i). This finding suggested that the sensor is capable of effectively monitoring swallowing at the throat when volunteers drink water, which provides a practical technological basis for augmenting traditional rehabilitation methods. With further clinical trials and research, this technique will be applied more effectively in the treatment and care of patients with dysphagia in the future [62]. The sensor also responded differently to different resistances depending on the different pronunciations of the word (CNF, CNT, SUST) (Fig. 6g). This is because the sensor responds to the deformation caused by different vibrations of the vocal folds, which enables speech recognition through the weak deformation generated by the movement of the vocal fold muscle groups when the human body pronounces a sound and highlights its application in speech-assisted output systems. The sensor adhered to the wrist can accurately observe three typical wave peaks of the human pulse, namely, the shock wave (P), tidal wave (T), and diastolic wave (D), and the pulse rate of the volunteer was calculated to be 65 beats per minute [63] (Fig. 6h). This kind of real-time acquisition of pulse rate data is an important indicator for cardiovascular disease monitoring [64]. All the above sensing performances showed good reproducibility, stability, and durability.

Conclusions

In summary, a strategy for efficiently dispersing CNTs while obtaining high-performance CCNT conductive materials has been developed based on natural CNFs. The biobased CCNT ink with a dispersion concentration of 60 wt% CNTs remains stably dispersed and demonstrates the printability of a variety of printing processes and substrates for facile realization of printed electronics. Benefiting from the ability of CNFs to adhere to the CNT surface, the CCNT composite films were assembled in an in-plane orientation, providing high electrical conductivity (67 S cm^{-1}) and good mechanical properties (153 MPa). As a proof of concept, CCNT-based multifunctional sensors and wearable electronics, e.g., piezoresistive sensors, deformation sensors, breath sensors, electrothermal sensors and electrochemical sensors, were fabricated and investigated for their excellent performance in monitoring human health. Based on the facile preparation, good biocompatibility, and versatile applications of these materials, we foresee that the development of advanced CCNT composites may promote the application of CNTs in advanced wearable devices. In conclusion, this work provides a theoretical basis

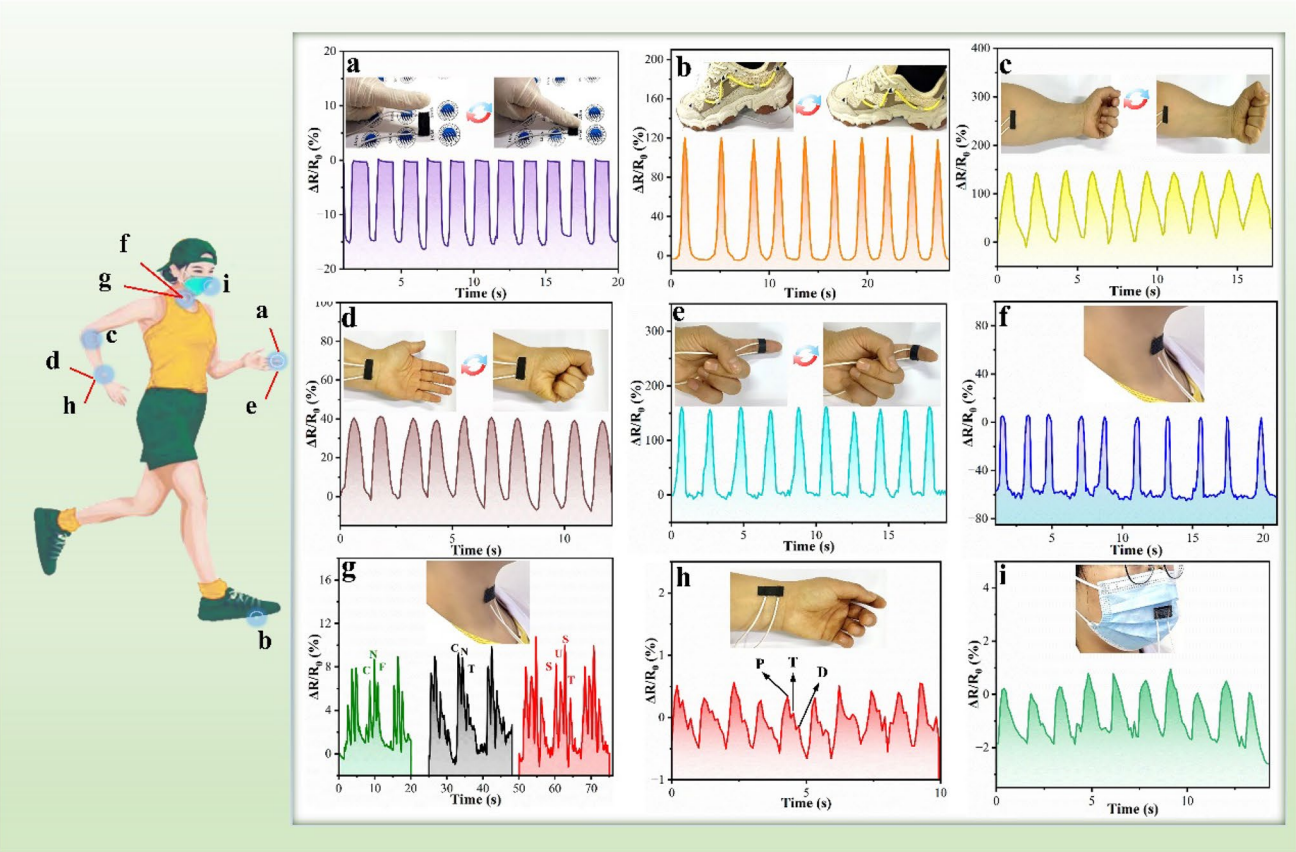

Fig. 6 Applications of wearable CCNT-based strain/pressure sensors for human motion detection, human physical signal collection and E-skin detection. Real-time recording of various human motions and human physical signals, including **a** wrist pulse, **b** respiration, **c** swallowing, **d** speaking, **e** touching, **f** walking, **g** bending, **h** making a fist, and **i** bending of the elbow

and experimental foundation for the development and design of active materials in the field of flexible electronics.

Supplementary Information The online version contains supplementary material available at https://doi.org/10.1007/s42765-024-00388-7.

Acknowledgements This work was supported by the International Joint Research Center for Biomass Chemistry and Materials, Shaanxi International Science and Technology Cooperation Base (2018GHJD-19), Shaanxi Key Industry Innovation Chain Projects (2020ZDLGY11-03), the National Natural Science Foundation of China (22378247), and the Shaanxi Qin Chuangyuan Project of "Scientist + Engineer" team construction (2022KXJ-135): a team of "scientists + engineers" of fibre-based biofilter plates. The authors would like to thank Prof. Xincun Dou of the Xinjiang Key Laboratory of Trace Chemicals Sensing of Xinjiang Technical Institute of Physics and Chemistry, CAS, for helpful discussions on topics related to this work.

Data availability The authors declare that the data supporting the findings of this study are available within the paper and its Supplementary Information files.

Declarations

Conflict of interest No potential conflicts of interest were reported by the authors.

References

1. Chen C, Feng J, Li J, Guo Y, Shi X, Peng H. Functional fiber materials to smart fiber devices. *Chem Rev*. **2022**;*123*:613–62.
2. Lin M, Hu H, Zhou S, Xu S. Soft wearable devices for deep-tissue sensing. *Nat Rev Mater*. **2022**;*7*:850–69.
3. Zhao D, Zhu Y, Cheng W, Chen W, Wu Y, Yu H. Cellulose-based flexible functional materials for emerging intelligent electronics. *Adv Mater*. **2021**;*33*: e2000619.
4. Owens CE, Headrick RJ, Williams SM, Fike AJ, Pasquali M, McKinley GH, Hart AJ. Substrate-versatile direct-write printing of carbon nanotube-based flexible conductors, circuits, and sensors. *Adv Func Mater*. **2021**;*31*:2100245.
5. Qiao L, Du K. Scalable production of high-quality carbon nanotube dispersion in aqueous solution using cellulose as dispersant by a freezing/thawing process. *J Colloid Interface Sci*. **2022**;*623*:1200–9.
6. Zhang S, Hua C, He B, Chang P, Du M, Liu Y. High-conductivity, stable Ag/cellulose paper prepared via in situ reduction of fractal-structured silver particles. *Carbohydr Polym*. **2021**;*262*: 117923.
7. Kinloch IA, Suhr J, Lou J, Young RJ, Ajayan PM. Composites with carbon nanotubes and graphene. An outlook. *Science*. **2018**;*362*:547–53.
8. Rivadeneyra A, Marín-Sánchez A, Wicklein B, Salmerón JF, Castillo E, Bobinger M, Salinas-Castillo A. Cellulose nanofibers as substrate for flexible and biodegradable moisture sensors. *Compos Sci Technol*. **2021**;*208*: 108738.

9. Alam MN, Kumar V, Lee D-J, Choi J. Synergistically toughened silicone rubber nanocomposites using carbon nanotubes and molybdenum disulfide for stretchable strain sensors. *Compos Part B-Eng*. **2023**;*259*: 110759.
10. Xu T, Du H, Liu H, Liu W, Zhang X, Si C, Liu P, Zhang K. Advanced nanocellulose-based composites for flexible functional energy storage devices. *Adv Mater*. **2021**;*33*:2101368.
11. Lyu S, Chang H, Zhang L, Wang S, Li S, Lu Y, Li S. High specific surface area MXene/SWCNT/cellulose nanofiber aerogel film as an electrode for flexible supercapacitors. *Compos Part B-Eng*. **2023**;*264*: 110888.
12. Zhao D, Liu R, Luo C, Guo Y, Hou C, Zhang Q, Li Y, Jia W, Wang H. Dielectrophoretic assembly of carbon nanotube chains in aqueous solution. *Adv Fiber Mater*. **2021**;*3*:312.
13. Gao C, Guo M, Liu Y, Zhang D, Gao F, Sun L, Li J, Chen X, Terrones M, Wang Y. Surface modification methods and mechanisms in carbon nanotubes dispersion. *Carbon*. **2023**;*212*: 118113.
14. Miyashiro D, Hamano R, Umemura K. A review of applications using mixed materials of cellulose, nanocellulose and carbon nanotubes. *Nanomaterials (Basel)*. **2020**;*10*:186.
15. Yoon H, Thompson R, Hwang B. Dispersibility study of carbon nanotubes using multiple light scattering: a mini-review. *J Colloid Interface Sci*. **2023**;*52*: 100686.
16. Rennhofer H, Zanghellini B. Dispersion state and damage of carbon nanotubes and carbon nanofibers by ultrasonic dispersion: a review. *Nanomaterials (Basel)*. **2021**;*11*:1469.
17. Oh S-H, Altug H, Jin X, Low T, Koester SJ, Ivanov AP, Edel JB, Avouris P, Strano MS. Nanophotonic biosensors harnessing van der Waals materials. *Nat Commun*. **2021**;*12*:3824.
18. Karousis N, Tagmatarchis N, Tasis D. Current progress on the chemical modification of carbon nanotubes. *Chem Rev*. **2010**;*110*:5366–97.
19. Xu S, Zhang Y, Zhu Y, Wu J, Li K, Lin G, Li X, Liu R, Liu X, Wong C-P. Facile one-step fabrication of glucose oxidase loaded polymeric nanoparticles decorating MWCNTs for constructing glucose biosensing platform: structure matters. *Biosens Bioelectron*. **2019**;*135*:153–9.
20. Zhang D, Song W, Lv L, Gao C, Gao F, Guo H, Diao R, Dai W, Niu J, Chen X, Wei J, Terrones M, Wang Y. Mono-dispersion decorated ultra-long single-walled carbon nanotube/aramid nanofiber for high-strength electromagnetic interference shielding film with Joule heating properties. *Carbon*. **2023**;*214*: 118315.
21. Liu L, Chang D, Gao C. A review of multifunctional nanocomposite fibers: design, preparation and applications. *Adv Fiber Mater*. **2023**;*3*:1–38.
22. Hajian A, Lindstrom SB, Pettersson T, Hamedi MM, Wagberg L. Understanding the dispersive action of nanocellulose for carbon nanomaterials. *Nano Lett*. **2017**;*17*:1439–47.
23. Zeng Z, Wang C, Wu T, Han D, Luković M, Pan F, Siqueira G, Nyström G. Nanocellulose assisted preparation of ambient dried, large-scale and mechanically robust carbon nanotube foams for electromagnetic interference shielding. *J Mater Chem A*. **2020**;*8*:17969–79.
24. Thakur A, Devi P. Paper-based flexible devices for energy harvesting, conversion and storage applications: a review. *Nano Energy*. **2022**;*94*: 106927.
25. Feng X, Wang X, Zhang C, Dang C, Chen Y, Qi H. Highly conductive and multifunctional nanocomposites based on sulfated nanocellulose-assisted high dispersion limit of single-walled carbon nanotubes. *Carbon*. **2021**;*183*:187–95.
26. De France K, Zeng Z, Wu T, Nystrom G. Functional materials from nanocellulose: utilizing structure-property relationships in bottom-up fabrication. *Adv Mater*. **2021**;*33*: e2000657.
27. Li Y, Zhu H, Wang Y, Ray U, Zhu S, Dai J, Chen C, Fu K, Jang SH, Henderson D, Li T, Hu L. Cellulose-nanofiber-enabled 3D printing of a carbon-nanotube microfiber network. *Small Methods*. **2017**;*1*:1700222.
28. Liu Y, Zhang S, Lin R, Li L, Li M, Du M, Tang R. Potassium permanganate oxidation as a carboxylation and defibrillation method for extracting cellulose nanofibrils to fabricate films with high transmittance and haze. *Green Chem*. **2021**;*23*:8069–78.
29. Liu Y, Zhang S, Li L, Coseri S. Cellulose nanofiber extraction from unbleached kraft pulp for paper strengthening. *Cellulose*. **2023**;*3*:3219–35.
30. Humphrey W, Dalke A, Schulten K. VMD: visual molecular dynamics. *J Mol Graph Model*. **1996**;*14*:33–8.
31. Daicho K, Saito T, Fujisawa S, Isogai A. Crystallinity of nanocellulose: dispersion-induced disordering of the grain boundary in biologically structured cellulose. *ACS Appl Nano Mater*. **2018**;*1*:5774–85.
32. Van Der Spoel D, Lindahl E, Hess B, Groenhof G, Mark AE, Berendsen HJC. GROMACS: Fast, flexible, and free. *J Comput Chem*. **2005**;*26*:1701–18.
33. Essmann U, Perera L, Berkowitz ML, Darden T, Lee H, Pedersen LG. A smooth particle mesh Ewald method. *J Chem Phys*. **1995**;*103*:8577–93.
34. Kirschner KN, Yongye AB, Tschampel SM, González-Outeiriño J, Daniels CR, Foley BL, Woods RJ. GLYCAM06: a generalizable biomolecular force field. *J Comput Chem*. **2008**;*29*:622–55.
35. Wang J, Wolf RM, Caldwell JW, Kollman PA, Case DA. Development and testing of a general amber force field. *J Comput Chem*. **2004**;*25*:1157–74.
36. Jorgensen WL. Monte Carlo simulation of n-butane in water. Conformational evidence for the hydrophobic effect. *J Chem Phys*. **1982**;*77*:5757–65.
37. Caddeo C, Pucci L, Gabriele M, Carbone C, Fernandez-Busquets X, Valenti D, Pons R, Vassallo A, Fadda AM, Manconi M. Stability, biocompatibility and antioxidant activity of PEG-modified liposomes containing resveratrol. *Int J Pharm*. **2018**;*538*:40–7.
38. Abo-Hamad A, Hayyan M, AlSaadi MA, Mirghani MES, Hashim MA. Functionalization of carbon nanotubes using eutectic mixtures: a promising route for enhanced aqueous dispersibility and electrochemical activity. *Chem Eng J*. **2017**;*311*:326–39.
39. Bratko D, Jönsson B, Wennerström H. Electrical double layer interactions with image charges. *Chem Phys Lett*. **1986**;*168*:449–54.
40. Fujisawa S, Okita Y, Fukuzumi H, Saito T, Isogai A. Preparation and characterization of TEMPO-oxidized cellulose nanofibril films with free carboxyl groups. *Carbohydr Polym*. **2011**;*84*:579–83.
41. Li C, Guo J, Jiang T, Zhang X, Xia L, Wu H, Guo S, Zhang X. Extensional flow-induced hybrid crystalline fibrils (shish) in CNT/PLA nanocomposite. *Carbon*. **2018**;*129*:720–9.
42. Singh D, Rawal A. Tensile mechanics of buckypaper: bridging the disconnect between disordered structure and carbon nanotube properties. *Carbon*. **2022**;*190*:299–311.
43. Zhu P, Kuang Y, Wei Y, Li F, Ou H, Jiang F, Chen G. Electrostatic self-assembly enabled flexible paper-based humidity sensor with high sensitivity and superior durability. *Chem Eng J*. **2021**;*404*: 127105.
44. Fang D, Zhou J, Sheng L, Tang W, Tang J. Juglone bonded carbon nanotubes interweaving cellulose nanofibers as self-standing membrane electrodes for flexible high energy supercapacitors. *Chem Eng J*. **2020**;*396*: 125325.
45. Huang H-D, Liu C-Y, Zhang L-Q, Zhong G-J, Li Z-M. Simultaneous reinforcement and toughening of carbon nanotube/cellulose conductive nanocomposite films by interfacial hydrogen bonding. *ACS Sustain Chem Eng*. **2015**;*3*:317–24.
46. Lin F, Wang Z, Chen J, Lu B, Tang L, Chen X, Lin C, Huang B, Zeng H, Chen Y. A bioinspired hydrogen bond crosslink strategy

toward toughening ultrastrong and multifunctional nanocomposite hydrogels. *J Mater Chem B*. **2020**;*8*:4002–15.
47. Sun Z, Zheng B, Chen C, Dong Z, Ma P. Synergistically enhancing weavability and interface behavior by applying PDMS/MXene on carbon fiber surface through ultrasound assistance. *Compos Part B Eng*. **2023**;*267*: 111071.
48. Huang YY, Terentjev EM. Dispersion of carbon nanotubes: mixing, sonication, stabilization, and composite properties. *Polymers*. **2012**;*4*:275–95.
49. Batista CA, Larson RG, Kotov NA. Nonadditivity of nanoparticle interactions. *Science*. **2015**;*350*:1242477.
50. Fukui T, Garcia-Hernandez JD, MacFarlane LR, Lei S, Whittell GR, Manners I. Seeded self-assembly of charge-terminated poly(3-hexylthiophene) amphiphiles based on the energy landscape. *J Am Chem Soc*. **2020**;*142*:15038–48.
51. Li C, Lan C, Guo M, Wang N, Ma Y. Wicking-driven evaporation self-assembly of carbon nanotubes on fabrics: generating controlled orientational structures. *Langmuir*. **2020**;*36*:13963–70.
52. Pritchard CQ, Funk G, Owens J, Stutz S, Gooneie A, Sapkota J, et al. Adjustable film properties of cellulose nanofiber and cellulose nanocrystal composites. *Carbohydr Polym*. **2022**;*286*: 119283.
53. Guan QF, Han ZM, Yang KP, Yang HB, Ling ZC, Yin CH, Yu SH. Sustainable double-network structural materials for electromagnetic shielding. *Nano Lett*. **2021**;*21*:2532–7.
54. Goetz LA, Naseri N, Nair SS, Karim Z, Mathew AP. All cellulose electrospun water purification membranes nanotextured using cellulose nanocrystals. *Cellulose*. **2018**;*25*:3011–23.
55. Gu X, Fan Q, Yang F, Cai L, Zhang N, Zhou W, Zhou W, Xie S. Hydro-actuation of hybrid carbon nanotube yarn muscles. *Nanoscale*. **2016**;*8*:17881–6.
56. Dai S, Chu Y, Liu D, Cao F, Wu X, Zhou J, Zhou B, Chen Y, Huang J. Intrinsically ionic conductive cellulose nanopapers applied as all solid dielectrics for low voltage organic transistors. *Nat Commun*. **2018**;*9*:2737.
57. Liu Y, Zhang S, Hua C, Li N, Li L. Silver-based conductive films on the filter paper template with the interfacial aid of PEI. *Cellulose*. **2023**;*30*:509–24.
58. Cui Y, He X, Liu W, Zhu S, Zhou M, Wang Q. Highly stretchable, sensitive, and multifunctional thermoelectric fabric for synergistic-sensing systems of human signal monitoring. *Adv Fiber Mater*. **2023**;*13*:1–11.
59. Wang L, Zhang M, Yang B, Ding X, Tan J, Song S, Nie J. Flexible, robust, and durable aramid fiber/CNT composite paper as a multifunctional sensor for wearable applications. *ACS Appl Mater Inter*. **2021**;*13*:5486–97.
60. Wang Q, Sheng H, Lv Y, Liang J, Liu Y, Li N, Xie E, Su Q, Ershad F, Lan W, Wang J, Yu C. A skin-mountable hyperthermia patch based on metal nanofiber network with high transparency and low resistivity toward subcutaneous tumor treatment. *Adv Funct Mater*. **2022**;*32*:2111228.
61. Ji F, Sun Z, Hang T, Zheng J, Li X, Duan G, Zhang C, Chen Y. Flexible piezoresistive pressure sensors based on nanocellulose aerogels for human motion monitoring: a review. *Compos Commun*. **2022**;*35*: 101351.
62. Kang YJ, Arafa HM, Yoo JY, Kantarcigil C, Kim JT, Jeong H, Yoo S, Oh S, Kim J, Wu C, Tzavelis A, Wu Y, Kwon K, Winograd J, Xu S, Martin-Harris B, Rogers JA. Soft skin-interfaced mechano-acoustic sensors for real-time monitoring and patient feedback on respiratory and swallowing biomechanics. *NPJ Digit Med*. **2022**;*5*:147.
63. Huang J, Li D, Zhao M, Ke H, Mensah A, Lv P, Tian X, Wei Q. Flexible electrically conductive biomass-based aerogels for piezoresistive pressure/strain sensors. *Chem Eng J*. **2019**;*373*:1357–66.
64. Fu Y, Zhao S, Wang L, Zhu R. A Wearable sensor using structured silver-particle reinforced PDMS for radial arterial pulse wave monitoring. *Adv Healthc Mater*. **2019**;*8*: e1900633.